Hindawi
International Journal of RF and Microwave Computer-Aided Engineering
Volume 2023, Article ID 9930037, 9 pages
https://doi.org/10.1155/2023/9930037

Research Article

High-Temperature Measurement Technology for Microwave Surface Resistance of Metal Materials

Chunmao Xie,[1,2] **Yunpeng Zhang**,[1] **Xue Niu**,[1] **Ming Huang**,[2] **Chong Gao**,[1] **Chengyong Yu**,[1] **Hu Zheng**,[1] **and En Li**[1]

[1]*School of Electronic Science and Engineering, University of Electronic Science and Technology of China, Chengdu 611731, China*
[2]*Southwest China Institute of Electronic Technology, Chengdu 610036, China*

Correspondence should be addressed to Yunpeng Zhang; zyp_ee@163.com

Received 28 June 2023; Revised 18 October 2023; Accepted 1 November 2023; Published 21 November 2023

Academic Editor: Giacomo Muntoni

The resonant cavity method is a commonly used method for high-temperature testing of the complex permittivity of dielectric materials. When a resonant cavity is used for high-temperature testing, the microwave surface resistance of the cavity metal material will deteriorate due to factors such as oxidation reaction and thermal fatigue, resulting in a decrease in testing accuracy and repeatability. Therefore, when designing a high-temperature resonant cavity, the temperature response characteristics of the microwave surface resistance of the cavity metal material should be obtained in advance. In this paper, a high-temperature measurement method of microwave surface resistance of metal materials based on a separate cylindrical resonator is proposed, a mathematical model of microwave surface resistance inversion based on the resonator quality factor is established, and a high-temperature measurement system of microwave surface resistance is integrated. The reliability of the proposed method and system is verified through simulation and experiment. The measurement frequency covers 7-18 GHz, and the maximum test temperature reaches 500°C. Systematic error of microwave surface resistance measurement at room temperature is less than 3%.

1. Introduction

High-temperature dielectric materials are widely used in fields such as aerospace [1], microwave metallurgy [2], and energy storage [3]. As an important link to evaluate the performance of high-temperature dielectric materials, accurate extraction of the high-temperature complex permittivity is a prerequisite and key to the design and application of high-temperature dielectric materials.

Many methods have been proposed for the measurement of the high-temperature complex permittivity of dielectric materials, and the open-ended coaxial probe method [4], free space method [5], waveguide method [6, 7], and cavity resonant method [8–11] are the primary measurement methods employed for cases over 1000°C. Compared to room temperature testing, high-temperature testing has more thermoelectric stability issues [12], and the performance change of the test fixture with the temperature has more contribution to the test error. For example, when using a resonant cavity to test the high-temperature complex permittivity of materials, the microwave surface resistance (MSR) of the cavity metal material will decline due to factors such as oxidation reaction and thermal fatigue, which will lead to the deterioration of the cavity resonant parameters (resonant frequency and quality factor) and ultimately lead to the decline of testing accuracy and repeatability of the cavity. Therefore, when designing a resonant cavity for high-temperature testing, in order to select suitable metal materials and estimate the variation of MSR with temperature, it is necessary to study methods for measuring the MSR of metal materials and establish corresponding testing systems, so the basic data on the thermoelectric performance of the cavity material can be obtained for the design of high-temperature testing fixtures.

Since the MSR determines the metal power loss and the metal power loss is closely related to the quality factor of the

microwave resonator, the MSR can be calculated based on the measurement of the quality factor of the resonator. At present, hollow resonant cavities [13–15] and dielectric resonators [16–19] are mainly used for the MSR measurement. For the former, part of the cavity wall is replaced with a metal under test (MUT), and the change in quality factor of the cavity before and after replacement can be used to extract the MSR of the MUT. For the latter, a low loss cylindrical medium (such as a sapphire) is placed on a single MUT plate (open-ended) or between two MUT plates (Hakki-Coleman's geometry), and the MSR of the MUT plate is calculated according to the measured quality factor and the known complex permittivity of the cylindrical medium; these methods have been widely used in the measurement of the MSR of graphene sheets, superconducting films, semiconductors, and copper clad laminates [19–23]. However, the above methods and systems are all used to measure the MSR of metal materials at room temperature, and there are currently no reports of high-temperature MSR measurement in the literature.

In this paper, a high-temperature measurement method of the MSR of metal materials based on a separate cylindrical resonator is proposed, and a mathematical model of the MSR inversion from the cavity quality factor is established. A test system is built; its test frequency covers 7-18 GHz, and the maximum test temperature reaches 500°C. The reliability of the proposed method and system is verified through simulation and experiment.

2. Measurement Theory

2.1. Inversion Formula. This paper proposes a high-temperature measurement method for the MSR of metal materials based on a separated cylindrical resonant cavity. In order to establish the relationship between the MSR and the cavity quality factor, it is necessary to make the MUT become a part of the cavity. At the same time, in order to facilitate testing operations, it is necessary to make the MUT easy to disassemble. Considering that the MUT is easily processed into a flat plate, which is suitable as a cover plate of the resonant cavity, the cylindrical cavity is improved to a separate cylindrical cavity; its upper cover plate and side wall are integrated (named main chamber), and the lower cover plate is composed of the MUT. During testing, the main chamber is inverted onto the MUT to form a complete cylindrical resonant cavity.

Using TE_{01p} mode for testing, the electric field energy at the lower cover plate is weak, so a small gap can be left between the main chamber and the MUT without greatly affecting the resonant performance of the cavity. This makes it easy to take and place the MUT, and thermal separation can be achieved between the MUT and the main chamber, which is beneficial for conducting high-temperature testing. The schematic diagram of the separated cylindrical resonant cavity is shown in Figure 1, where the inner diameter and inner length of the cavity are $2a$ and L, respectively. The field in the cavity is excited and extracted by two coupling ports from the upper cover plate.

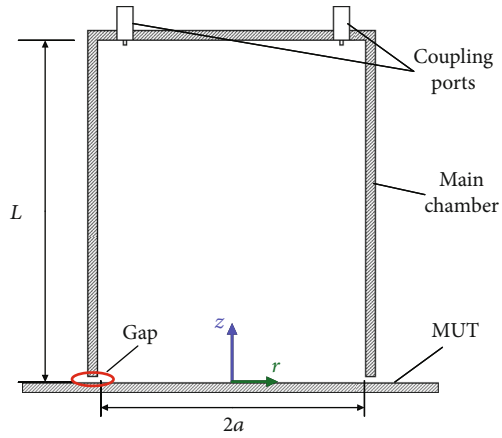

Figure 1: Schematic diagram of separated cylindrical resonant cavity.

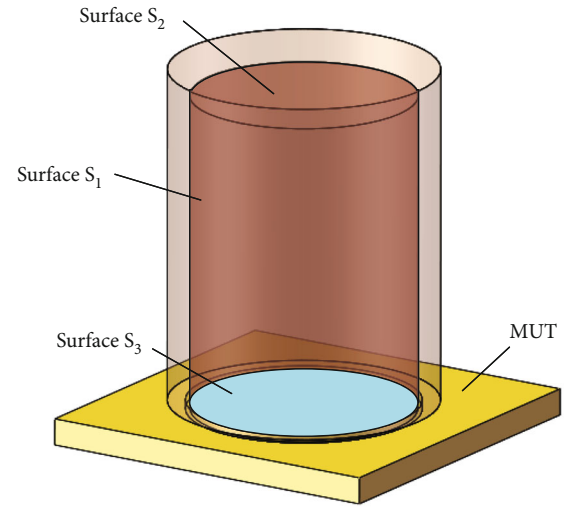

Figure 2: Metal loss distribution in the separated cylindrical resonant cavity.

For the TE_{01p} testing mode, the expression of the cavity field is as follows:

$$\begin{cases} H_r = H_0 \dfrac{\beta a}{u'_{01}} J'_0\left(\dfrac{u'_{01}}{a} r\right) \cos \beta z, \\ H_z = H_0 J_0\left(\dfrac{u'_{01}}{a} r\right) \sin \beta z, \\ E_\varphi = jH_0 k\eta \dfrac{a}{u'_{01}} J'_0\left(\dfrac{u'_{01}}{a} r\right) \sin \beta z, \\ E_r = E_z = H_\varphi = 0, \end{cases} \tag{1}$$

where $\beta = p\pi/L$, $\eta = \sqrt{\mu/\varepsilon}$, $k = \omega\sqrt{\mu\varepsilon}$, μ and ε are the complex permeability and complex permittivity of the filled medium (air in this paper) in the cavity, ω is the angular frequency, H_0 is the coefficient determined from the boundary

Table 1: Resonant frequency and quality factor of cylindrical resonant cavity with different gap width (corresponding to σ_1).

Mode	Gap width (mm)					
	f (MHz)			Q		
	0	0.5	1	0	0.5	1
TE_{011}	7595.77	7595.69	7595.69	27096	27100	27100
TE_{012}	8347.30	8347.35	8347.30	27195	27197	27196
TE_{013}	9468.31	9468.34	9468.30	27696	27699	27697
TE_{014}	10844.9	10844.9	10844.9	28593	28603	28601
TE_{015}	12391.8	12392.1	12392.2	29795	29790	29786
TE_{016}	14053.5	14053.9	14053.9	31134	31137	31133
TE_{017}	15793.3	15794.2	15794.3	32582	32566	32563
TE_{018}	17588.3	17589.8	17590.0	34051	34024	34022

Table 2: Resonant frequency and quality factor of cylindrical resonant cavity with different gap width (corresponding to σ_2).

Mode	Gap width (mm)					
	f (MHz)			Q		
	0	0.5	1	0	0.5	1
TE_{011}	7595.55	7595.59	7595.59	28355	28354	28354
TE_{012}	8347.19	8347.25	8347.25	31631	31629	31629
TE_{013}	9468.25	9468.35	9468.34	36174	36172	36170
TE_{014}	10844.8	10844.9	10844.9	41239	41234	41231
TE_{015}	12391.9	12392.2	12392.2	46349	46340	46337
TE_{016}	14053.6	14054.0	14054.0	51271	51260	51252
TE_{017}	15793.3	15794.3	15794.4	55947	55908	55902
TE_{018}	17588.3	17590.0	17590.1	60317	60269	60267

Table 3: R_{s3} calculated by quality factors under different gaps and their comparison with theoretical MSR (unit: mΩ).

Mode	TE_{011}	TE_{012}	TE_{013}	TE_{014}	TE_{015}	TE_{016}	TE_{017}	TE_{018}
R_{s3-T}	77.4	81.1	86.4	92.5	98.9	105.3	111.7	117.9
R_{s3-0}	78.7	82.9	87.2	93.0	99.1	105.5	111.7	117.8
R_{s3-1}	78.4	82.9	87.2	92.9	99.1	105.5	111.8	118.0

conditions, $J_0'(x)$ is the derivative of the first kind of the Bessel function, and u_{01}' is the first root of $J_0'(x)$.

When the resonant cavity reaches the resonant state, the magnetic field energy is equal to the electric field energy, and the energy storage expression is

$$W = \frac{\varepsilon}{2}\int_{z=0}^{L}\int_{\varphi=0}^{2\pi}\int_{r=0}^{a}\left|E_\varphi\right|^2 r dr d\varphi dz. \tag{2}$$

When measuring the MSR of the MUT, there is no dielectric loss, only the metal loss P_c of the cavity wall needs to be considered. In addition, the resonant cavity adopts weak coupling; it can be considered that the measured loaded quality factor Q_u of the cavity is approximately equal to the unloaded quality factor Q_c, which is given by

$$Q_u \approx Q_c = \omega\frac{W}{P_c}. \tag{3}$$

P_c is related to the MSR and magnetic field components along the tangential direction of the cavity wall, and its expression is

$$P_c = \frac{R_s}{2}\oint_S |J_s|^2 ds = \frac{R_s}{2}\oint_S |H_{\tan}|^2 ds, \tag{4}$$

where J_s represents the cavity wall current, $H_{\tan}$ represents the tangential magnetic field component along the cavity wall, and R_s represents the MSR of the cavity wall. P_c comes from the loss P_{c1} of the surface S_1 on the side wall, the loss P_{c2} of the surface S_2 on the upper cover plate, and the loss P_{c3} of the surface S_3 on the lower cover plate, as shown in Figure 2.

Table 4: Simulated quality factors of TE_{011} mode corresponding to different surface roughness.

Roughness (μm)	Q	R_{s3} (mΩ)
0	28354	31.5
1	28352	31.6
2	28220	37.0
3	26708	102.0
4	24186	228.7
5	21942	365.9
7	19060	589.4
9	17518	739.2
11	16623	838.9

By substituting the field expression of (1) into (4), the expressions for the losses of each cavity wall can be obtained as follows:

$$\begin{cases} P_{c1} = \dfrac{R_{s1}}{2}\displaystyle\int_{S_1} |H_z(r=a)|^2 ds, \\ P_{c2} = \dfrac{R_{s2}}{2}\displaystyle\int_{S_2} |H_r(z=L)|^2 ds, \\ P_{c3} = \dfrac{R_{s3}}{2}\displaystyle\int_{S_3} |H_r(z=0)|^2 ds, \end{cases} \tag{5}$$

where R_{s1}, R_{s2}, and R_{s3} represent the MSR of surfaces S_1, S_2, and S_3, respectively. Therefore, the loaded quality factor can be written as follows:

$$Q_u \approx \frac{\omega W}{P_{c1} + P_{c2} + P_{c3}}. \tag{6}$$

In actual testing, it is necessary to obtain R_{s1} and R_{s2} in advance, that is, to calibrate the system. In this paper, a flat plate with the same material and processing technology as the main chamber is used to form a resonant cavity with the main chamber. According to the measured Q_u, R_{s1} and R_{s2} can be calculated, and $R_{s1} = R_{s2}$.

Based on the calibrated R_{s1} and R_{s2}, R_{s3} of the MUT can be given by

$$R_{s3} = 2\frac{\omega - Q_u(P_{c1} + P_{c2})}{DQ_u}, \tag{7}$$

with

$$D = \int_{s_3} |H_r(z=0)|^2 ds. \tag{8}$$

2.2. Impact of Gap. To measure the MSR of the MUT at high temperatures, the MUT needs to be heated. To reduce the impact of high temperature on the main chamber, the main chamber is water-cooled, and the main chamber is lifted up by a small gap, as shown in Figure 1. Since TE_{01p} modes are used as the operating modes, their electric and magnetic fields at the outer edge of the bottom of the cavity are the weakest from (1). In addition, the air gap does not cut off

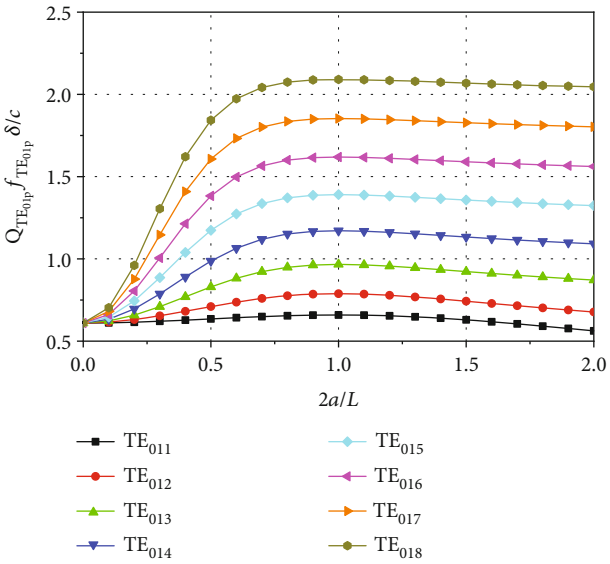

Figure 3: Q for cylindrical resonator TE_{01p} modes.

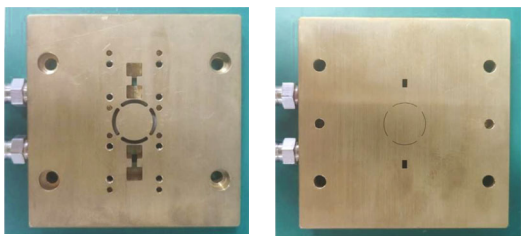

Figure 4: Coupling structure and annular gaps on the upper cover plate of the main chamber: (a) outer wall; (b) inner wall.

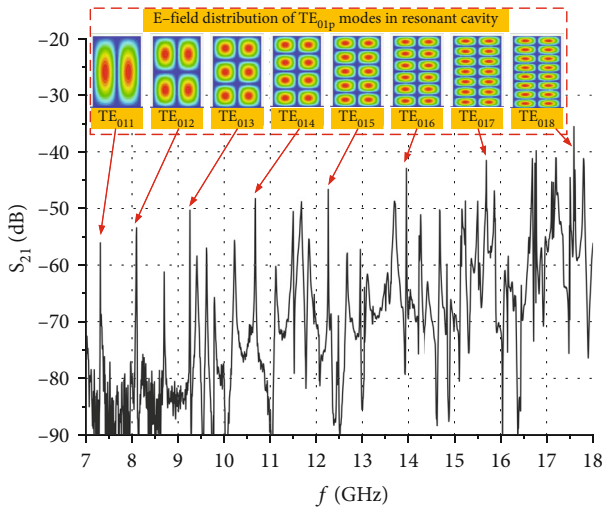

Figure 5: Measured resonant peak distribution within 7-18 GHz.

Table 5: Measured quality factor with and without gap.

Mode	TE_{011}	TE_{012}	TE_{013}	TE_{014}	TE_{015}	TE_{016}	TE_{017}	TE_{018}
Q_1	13449	15285	16821	19651	21521	22845	24741	25133
Q_2	13460	15305	16855	19692	21576	22911	24815	25214

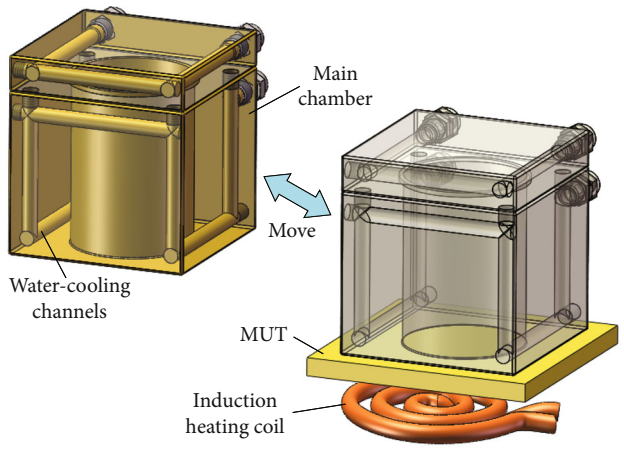

Figure 6: Proposed high-temperature testing system scheme.

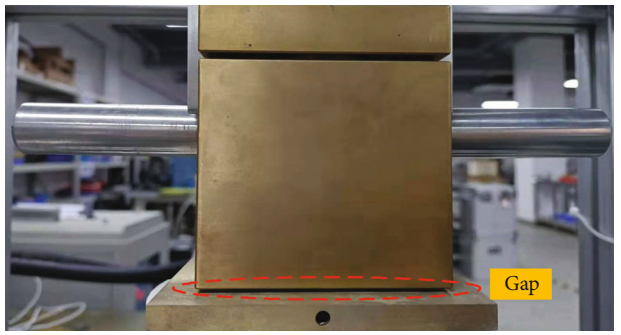

Figure 7: A gap between the main chamber and the MUT.

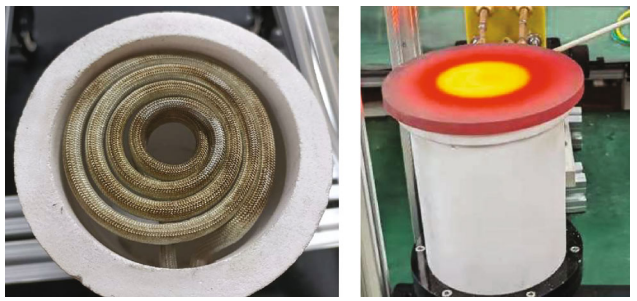

Figure 8: Photo and heating diagram of the induction coil.

the wall current of TE_{01p} modes. Therefore, the small air gap has little effect on the resonance performance of TE_{01p} modes.

In this paper, the impact of the air gap on testing is quantitatively analyzed by the electromagnetic simulation software Ansys HFSS. Cylindrical cavity models with and without gap are established, respectively, where a is set to 25 mm and L is set to 75 mm. For the cylindrical cavity

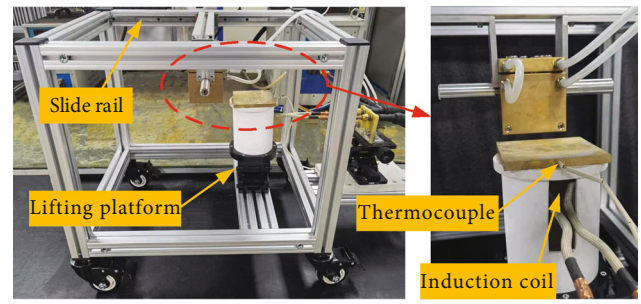

Figure 9: Photo of the integrated test system.

model with gap, the width of the gap is set to 0.5 mm and 1 mm, respectively. For the above dimensions, 8 operating modes (from TE_{011} mode to TE_{018} mode) of the cylindrical cavity can be distributed in the 7-18 GHz frequency band. The material of main chamber is set to gold (conductivity $\sigma = 4.1 \times 10^7$), and the conductivity of the MUT is set to σ_1 ($=5 \times 10^6$) and σ_2 ($=5 \times 10^7$), respectively. Based on the eigenmode solver, the resonant frequency f and quality factor Q of each operating mode with and without gap are simulated, respectively; results are given in Tables 1 and 2.

It can be seen that the change of resonant frequency and quality factor caused by the gap is very small. The maximum deviation of resonant frequency is 0.1‰, and the maximum deviation of quality factor is 0.9‰. In addition, for the MUT with conductivity σ_1, the formulas in Section 2.1 are used to calculate its MSR, and the inversion results based on the quality factor in Table 1 are obtained when there is no gap and the gap is 1 mm (represented by R_{s3-0} and R_{s3-1}, respectively), as shown in Table 3. Meanwhile, the theoretical MSR calculated based on σ_1 (represented by R_{s3-T} and $R_{s3-T} = \sqrt{\mu_s \omega / 2\sigma_1}$, where μ_s is the permeability of metals) is given in the table. It can be concluded that the relative error between the inversion results and the theoretical results is within 2.2%. Therefore, in actual testing, the gap between the main chamber and the MUT can be set to 1 mm, and the inversion model without considering the gap can still be used.

2.3. Impact of Roughness. The MSR of metal materials is not only affected by material conductivity but also by surface roughness. The difference between the peak and valley of surface fluctuations is called surface roughness. In this paper, the influence of roughness on the MSR inversion is analyzed through simulation. For the above model without the gap, the material of main chamber is still set to gold and its roughness is set to 0; the conductivity of the MUT is set to σ_2, and its roughness is changed from 0 to 11 μm. Simulated quality factors of TE_{011} mode corresponding to

Table 6: Resonant frequency, quality factor in calibration state, and calculated equivalent MSR of the main chamber.

Mode	TE_{011}	TE_{012}	TE_{013}	TE_{014}	TE_{015}	TE_{016}	TE_{017}	TE_{018}
f (GHz)	7.31	8.09	9.25	10.66	12.24	13.39	15.69	17.59
Q	13449	15285	16821	19651	21521	22845	24741	25133
R_{s-mc} (mΩ)	56.6	59.5	67.8	72.1	81.0	95.3	82.7	115.2

different surface roughness are shown in Table 4, and R_{s3} calculated based on Q is also given in the table.

From the table, it can be concluded that the surface roughness of metals has a significant impact on the MSR. When the surface roughness increases, the MSR significantly deviates from the theoretical value. This further shows that the MSR cannot be completely calculated by theory, and it is necessary to measure the MSR, especially when the material is worked at high temperature, where oxidation reaction and thermal fatigue will further deteriorate the metal surface states (roughness, attachment of reactants, etc.).

3. System Development

3.1. Design of Separate Cylindrical Resonator. To achieve broadband operation for a single resonator, a multimode cylindrical resonator is designed, which uses multiple TE_{01p} working modes. Expressions of the resonant frequency and the unloaded quality factor of the TE_{01p} mode are given by [24]

$$f_{TE_{01p}} = \frac{c}{2a}\sqrt{\left(\frac{u'_{01}}{\pi}\right)^2 + \left(\frac{pa}{L}\right)^2}, \tag{9}$$

$$Q_{TE_{01p}} = \frac{c}{f_{TE_{01p}}\delta}\frac{\left[\left(u'_{01}\right)^2 + ((p\pi/L)a)^2\right]^{3/2}}{2\pi\left[\left(u'_{01}\right)^2 + (2a/L)((p\pi/L)a)^2\right]}, \tag{10}$$

where c is the speed of light and δ is the skin depth, which depends on the frequency and the conductivity of the cavity material.

Figure 3 gives a plot of $Q_{TE_{01p}} f_{TE_{01p}} \delta/c$ against $2a/L$ for TE_{01p} mode ($p = 1, 2, \cdots, 8$); it can be seen that when $2a/L$ is between 0.6 and 1.5, the cylindrical resonator has a relatively high quality factor. In addition, from (9), when the radius a is fixed, the difference in resonant frequencies between two adjacent TE_{01p} modes increases with the increase of $2a/L$. Therefore, in order to form more operating modes within the required frequency band range, the value of $2a/L$ should not be too large. Based on the above analysis, the value of $2a/L$ in this paper is taken as 2/3. After optimization calculation, TE_{011}-TE_{018} modes are selected, and the resonant frequencies of the first and eighth modes are set around 7.5 GHz and 17.5 GHz, respectively, correspondingly, $a = 25$ mm and $L = 75$ mm.

The coupling structure is set on the upper cover plate of the main chamber, and coupling method is hole coupling, as shown in Figure 4. Two WRD650 standard double-ridge waveguides, which work in the 6.5-18 GHz frequency band, are used as feed transmission lines. Coupling coefficient is adjusted between -35 and -55 dB by optimizing the aperture and depth of the coupling holes. For this situation, the unloaded quality factor is approximately equal to the loaded quality factor.

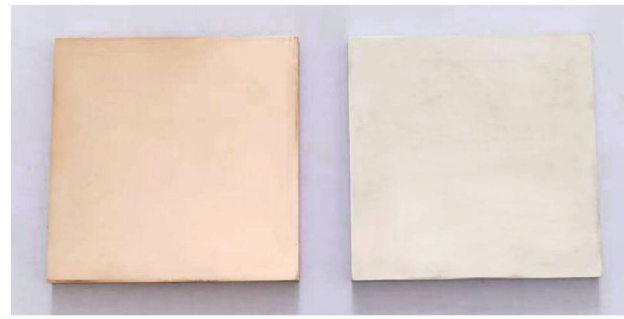

(a) (b)

Figure 10: Photo of the polished copper plate (a) and aluminum plate (b).

In addition, for the interference modes, annular gaps are a kind of effective structure for the interference mode suppression [25, 26]. In this paper, annular gaps are designed on the upper cover plate, as shown in Figure 4. For TE_{01p} modes, due to the circumferential distribution of wall current, the introduction of annular gaps does not have a significant impact on the TE_{01p} modes. While for other modes with radial wall current distribution, the annular gaps can cut off their wall current and disrupt their resonance conditions, so the effect of suppressing partial interference modes is achieved. The main chamber is machined with brass, by combining the main chamber with a large brass plate to form a cylindrical resonator; measured resonant peak distribution within 7-18 GHz is given in Figure 5. It can be seen that TE_{01p} modes are far away from residual interference modes, so the working modes are pure. Moreover, measured quality factor with and without gap (denoted by Q_1 and Q_2, respectively) is given in Table 5, where the gap width is set to 1 mm. It can be seen that the gap does not cause significant quality factor deterioration, and its maximum reduction was 0.32%.

3.2. Test System Integration. Test system scheme is proposed in Figure 6. When heating the MUT, a planar induction coil is placed below the MUT to achieve heating at the bottom of the MUT, while the main chamber is moved away. When the MUT is heated to the desired temperature, the main chamber is moved back to the upper side of the MUT. At this time, the main chamber and the MUT form a complete TE_{01p} mode cylindrical resonator.

Table 7: Measured and theoretical MSR of copper and aluminum plates (unit: mΩ).

	Mode	TE_{011}	TE_{012}	TE_{013}	TE_{014}	TE_{015}	TE_{016}	TE_{017}	TE_{018}
Copper	R_{s-t}	22.3	23.5	25.1	26.9	28.9	30.2	32.7	34.6
	R_{s-m}	22.2	23.6	25.2	27.3	29.1	31.0	32.1	35.4
Aluminum	R_{s-t}	27.9	29.3	31.3	33.6	36.0	37.7	40.8	43.2
	R_{s-m}	27.7	29.5	31.5	34.1	36.4	38.8	40.1	44.2

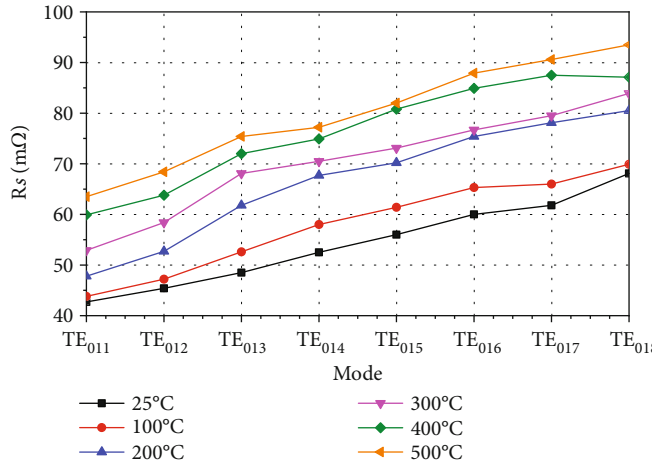

Figure 11: High-temperature test results of the MSR of a brass plate.

To avoid the impact of high temperature on the performance of the main chamber, water-cooling channels are designed in the side wall and upper cover plate of the main chamber, as shown in Figure 6. At the same time, the main chamber is lifted above the MUT and maintains a 1 mm gap with the upper surface of the MUT, as shown in Figure 7. These measures ensure that the temperature of the main chamber can be stabilized at room temperature, so it is only necessary to calibrate the MSR of the main chamber at room temperature.

The induction heating method is used to heat the MUT, which has the advantages of high efficiency, high safety, and good environmental adaptability. To achieve heating from the bottom, the induction coil is in a planar spiral shape; its photo and heating diagram are shown in Figure 8. The side wall of the MUT is drilled with a through-hole, which can be inserted into a thermocouple for the temperature measurement. The temperature uniformity of the test area can be obtained by changing the insertion depth of the thermocouple, and the temperature difference between the center and the edge of the test area is less than 30°C when it is heated up to 500°C. The integrated test system is shown in Figure 9 (the vector network analyzer and connecting cables are not shown in the figure). The main chamber is lifted and installed on the slide rails for easy movement and positioning.

4. Measurement Results and Discussion

4.1. Room Temperature Measurement. Considering the influence of surface roughness, coupling holes, annular gaps, and the gap between the main chamber and the MUT, it is necessary to calibrate the MSR (we call it equivalent MSR) of the main chamber before testing. Since the main chamber is water-cooled, its change in the MSR is negligible, and the calibration is only required at room temperature. This article uses a plate with the same material (brass) and processing technology as the main chamber for calibration. Table 6 gives the resonant frequency, quality factor in the calibration state, and equivalent MSR R_{s-mc} of the main chamber, which are calculated from (7), where $R_{s1} = R_{s2} = R_{s3}$. As a result, during testing, the calibrated R_{s-mc} is assigned to R_{s1} and R_{s2} in (5).

A copper plate and an aluminum plate processed by mirror polish (A3: Ra 0.032 μm) are used as the MUT, as shown in Figure 10. For these two samples, the influence of the surface roughness on the MSR can be ignored and material conductivity ($\sigma_{\text{copper}} = 5.8 \times 10^7$ and $\sigma_{\text{aluminum}} = 3.72 \times 10^7$) can be used to calculate the theoretical MSR ($R_s = \sqrt{\mu_s \omega / 2\sigma}$). Table 7 gives the MSR of the two MUTs measured at room temperature. It can be seen that the test results R_{s-m} and theoretical results R_{s-t} are in good agreement; the deviation between them is less than 3%. This indicates that accurate measurement of the MSR of the metal plate can be achieved by calibrating the MSR of the main chamber.

4.2. High-Temperature Measurement. The MSR of a brass plate is measured at high temperatures. The test temperature is set to 500°C considering the melting point of brass. Figure 11 shows the variation of the MSR of the brass plate with the temperature at eight operating modes. It can be seen that the MSR increases with increasing temperature, which is in accordance with the physical laws. For the metal,

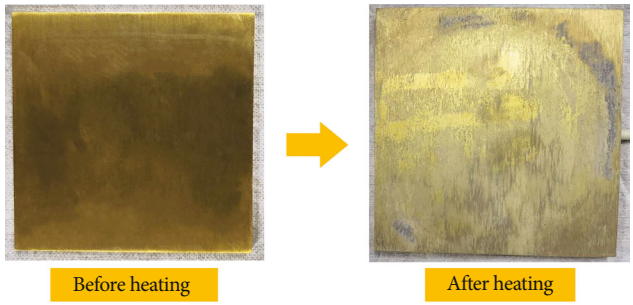

Figure 12: Comparison of the brass plate before and after heating.

heating intensifies the collision of free electrons with atomic cores, resulting in poorer conductivity and higher MSR. Therefore, when designing electronic devices for high-temperature scenarios (e.g., resonant cavities for high-temperature testing), it is important to consider the temperature coefficient of resistance of the metal material in addition to its room temperature conductivity. Moreover, due to the heating in the atmospheric environment, the oxidation of brass intensifies at high temperatures; the generated oxides adhere to the surface of the brass plate and are unevenly distributed, as shown in Figure 12, which also makes the MSR increase with the increase of the temperature.

5. Conclusion

In this paper, a high-temperature test method for the microwave surface resistance of metal materials based on a separate cylindrical resonator is proposed. A test model is established, a test sensor is designed, and a high-temperature test system is built for this method, which has the characteristics of convenient sample placement and retrieval and wide test frequency band. The reliability and accuracy of the proposed method and system are verified by simulation and physical testing. The research in this paper can provide strong technical support for the material selection and thermoelectric performance evaluation of high-temperature measurement sensors for dielectric materials.

Data Availability

The graph data used to support the findings of this study are included within the article.

Conflicts of Interest

The authors declare that they have no conflicts of interest.

Acknowledgments

This work was supported by the National Natural Science Foundation of China under Grant 62201130, Grant 62101108, Grant 62301134, and Grant U2241241.

References

[1] A. Nag, R. R. Rao, and P. K. Panda, "High temperature ceramic radomes (HTCR) - a review," *Ceramics International*, vol. 47, no. 15, pp. 20793–20806, 2021.

[2] E. R. Bobicki, C. A. Pickles, J. Forster, O. Marzoughi, and R. Hutcheon, "High temperature permittivity measurements of selected industrially relevant ores: review and analysis," *Minerals Engineering*, vol. 145, article 106055, 2020.

[3] X. J. Liu, M. S. Zheng, G. Chen, Z. M. Dang, and J. W. Zha, "High-temperature polyimide dielectric materials for energy storage: theory, design, preparation and properties," *Energy & Environmental Science*, vol. 15, no. 1, pp. 56–81, 2022.

[4] M. Arai, J. G. P. Binner, and T. E. Cross, "Comparison of techniques for measuring high-temperature microwave complex permittivity: measurements on an alumina/zircona system," *Journal of Microwave Power and Electromagnetic Energy*, vol. 31, no. 1, pp. 12–18, 1996.

[5] M. S. Hilario, B. W. Hoff, B. Jawdat et al., "*W*-band complex permittivity measurements at high temperature using free-space methods," *IEEE Transactions on Components, Packaging and Manufacturing Technology*, vol. 9, no. 6, pp. 1011–1019, 2019.

[6] A. E. Bogle, M. W. Hyde, M. J. Havrilla, and J. S. Sovern, "High-temperature RF material characterization using a dual-chambered rectangular waveguide fixture," *IEEE Transactions on Instrumentation and Measurement*, vol. 66, no. 9, pp. 2422–2427, 2017.

[7] G. Guo, E. Li, Z. Li, Q. Zhang, and F. He, "A test system for complex permittivity measurements of low-loss materials at high temperatures up to 2000° C," *Measurement Science and Technology*, vol. 22, no. 4, article 045707, 2011.

[8] E. Li, Z. P. Nie, G. Guo, Q. Zhang, Z. Li, and F. He, "Broadband measurements of dielectric properties of low-loss materials at high temperatures using circular cavity method," *Progress in Electromagnetics Research*, vol. 92, pp. 103–120, 2009.

[9] Y. Zhang, E. Li, J. Zhang, C. Yu, H. Zheng, and G. Guo, "A broadband variable-temperature test system for complex permittivity measurements of solid and powder materials," *Review of Scientific Instruments*, vol. 89, no. 2, article 024701, 2018.

[10] B. Garcia-Baños, J. Catalá-Civera, F. Peñaranda-Foix, P. Plaza-González, and G. Llorens-Vallés, "*In situ* monitoring of microwave processing of materials at high temperatures through dielectric properties measurement," *Materials*, vol. 9, no. 5, p. 349, 2016.

[11] Y. Zhou, E. Li, G. Guo, Y. Gao, and T. Yang, "Broadband complex permittivity measurement of low loss materials over large temperature ranges by stripline resonator cavity using segmentation calculation method," *Progress in Electromagnetics Research*, vol. 113, pp. 143–160, 2011.

[12] L. F. Chen, C. K. Ong, C. P. Neo, V. V. Varadan, and V. K. Varadan, *Microwave Electronics: Measurement and Materials Characterization*, John Wiley & Sons, Chichester, UK, 2004.

[13] B. A. Tonkin and Y. G. Proykova, "Microwave surface resistance of cuprate superconductors," *IEEE Transactions on Applied Superconductivity*, vol. 7, no. 2, pp. 1257–1259, 1997.

[14] R. Gumbleton, J. A. Cuenca, S. Hefford, K. Nai, and A. Porch, "Measurement technique for microwave surface resistance of additive manufactured metals," *IEEE Transactions on Microwave Theory and Techniques*, vol. 69, no. 1, pp. 189–197, 2021.

[15] M. P. Kirley, N. Carlsson, B. B. Yang, and J. H. Booske, "Study of the effect of surface roughness and skin depth on the conductivity of metals at 650 GHz," in *IVEC 2012*, pp. 239-240, Monterey, CA, USA, April 2012.

[16] C. Zeng, Z. Luo, S. Bu, K. Yang, and Q. Zhang, "A novel method for the measurement of frequency-character of surface resistance of HTS thin film," *Chinese Science Bulletin*, vol. 55, no. 11, pp. 1088–1091, 2010.

[17] S. Hefford, N. Clark, R. Gumbleton, and A. Porch, "Liftoff dielectric resonator for the microwave surface resistance measurement of metal plates," *IEEE Transactions on Instrumentation and Measurement*, vol. 70, pp. 1–8, 2021.

[18] C. Zeng, L. Chen, S. Bu, J. Ning, Q. Zhang, and Z. Wang, "Characterizing the distribution of microwave surface resistance of HTS film based on metal ring," *Journal of Superconductivity and Novel Magnetism*, vol. 32, no. 7, pp. 1903–1908, 2019.

[19] J. Mazierska and C. Wilker, "Accuracy issues in surface resistance measurements of high temperature superconductors using dielectric resonators (corrected)," *IEEE Transactions on Applied Superconductivity*, vol. 11, no. 4, pp. 4140–4147, 2001.

[20] M. V. Jacob, J. Mazierska, K. Leong, D. Ledenyov, and J. Krupka, "Surface resistance measurements of HTS thin films using SLAO dielectric resonator," *IEEE Transactions on Applied Superconductivity*, vol. 13, no. 2, pp. 2909–2912, 2003.

[21] J. Krupka, "Measurements of the surface resistance and the effective conductivity of copper cladded laminates employing dielectric resonator technique," in *2007 IEEE/MTT-S International Microwave Symposium*, pp. 515–518, Honolulu, HI, USA, June 2007.

[22] J. Krupka and J. Mazierska, "Contactless measurements of resistivity of semiconductor wafers employing single-post and split-post dielectric-resonator techniques," *IEEE Transactions on Instrumentation and Measurement*, vol. 56, no. 5, pp. 1839–1844, 2007.

[23] O. Shaforost, K. Wang, S. Goniszewski et al., "Contact-free sheet resistance determination of large area graphene layers by an open dielectric loaded microwave cavity," *Journal of Applied Physics*, vol. 117, no. 2, article 024501, 2015.

[24] R. E. Collin, *Foundations for Microwave Engineering*, Wiley-IEEE Press, New York, 2nd edition, 2000.

[25] T. Shimizu, S. Kojima, and Y. Kogami, "Accurate evaluation technique of complex permittivity for low-permittivity dielectric films using a cavity resonator method in 60-GHz band," *IEEE Transactions on Microwave Theory and Techniques*, vol. 63, no. 1, pp. 279–286, 2015.

[26] T. Shimizu, K. Takahagi, K. Ebisawa, and Y. Kogami, "Complex permittivity and uncertainty evaluations for an ultrathin photosensitive insulator film using a millimeter wave circular cavity resonator," in *2021 IEEE Asia-Pacific Microwave Conference (APMC)*, pp. 461–463, Brisbane, Australia, November 2021.